Failure at Frame-Stringer Intersections in PRSEUS Panels

Dawn Jegley

ABSTRACT

NASA, the Air Force Research Laboratory and The Boeing Company have worked to develop new low-cost, light-weight composite structures for aircraft. A Pultruded Rod Stitched Efficient Unitized Structure (PRSEUS) concept has been developed which offers advantages over traditional metallic structures. In this concept a stitched carbon-epoxy material system has been developed with the potential for reducing the weight and cost of transport aircraft structure by eliminating fasteners, thereby reducing part count and labor. By adding unidirectional carbon rods to the top of stiffeners, the panel becomes more structurally efficient. This combination produces a more damage tolerant design. This study focuses on the intersection between the rod-stiffener and the foam-filled frame in a PRSEUS specimen. Compression loading is considered, which induces stress concentrations at the intersection point that can lead to failures. An experiment with accompanying analysis for a single-frame specimen is described, followed by a parametric study of simple reinforcements to reduce strains in the intersection region.

INTRODUCTION

NASA, the Air Force Research Laboratory and The Boeing Company have worked to develop new low-cost, light-weight composite structures for aircraft. A Pultruded Rod Stitched Efficient Unitized Structure (PRSEUS) concept has been developed which offers advantages over traditional metallic structure [1]. In this concept a stitched carbon-epoxy material system has been developed with the potential for reducing the weight and cost of commercial transport aircraft structure. By stitching through the thickness of a dry carbon-epoxy material system, the labor associated with panel fabrication and assembly can be significantly reduced. When stitching through the thickness of pre-stacked skin, stringers, intercostals and spar caps before infusion, the need for mechanical fasteners is almost eliminated. This manufacturing approach reduces part count, and therefore, cost of the structure. In addition, stitching reduces delamination and improves damage tolerance, allowing for a lighter structure with more gradual failures than traditional composites. However, as with any structure, discontinuities will cause stress concentrations. One location of stress concentration is at the intersection of two perpendicular stiffeners [2].

Dawn C. Jegley, NASA Langley Research Center, mail stop 190 Hampton, Virginia 23681, U.S.A.

The PRSEUS concept consists of carbon-epoxy panels fabricated from dry components and then infused with VRM 34 resin in an oven while subjected to vacuum pressure. Skins, flanges, and webs are composed of layers of graphite material forms that are prekitted in multi-ply stacks using Hercules, Inc. AS4 fibers. Several stacks of the prekitted material are used to build up the desired thickness and configuration. The prekitted stacks had a $[45/-45/0_2/90/0_2/-45/45]_T$ laminate stacking sequence. Stack thickness was approximately 0.052 inches. Specimens are stitched together using Vectran fibers. Stiffener flanges are stitched to the skin and no mechanical fasteners are used for joining. To maintain the panel geometry during fabrication, first stiffeners and then the skin are placed in a stitching tool for assembly prior to moving to a curing tool for consolidation in the oven. The stiffeners running in one direction consist of webs with a unidirectional carbon fiber rod at the top of the web. The pultruded rods are Toray unidirectional T800 fiber with a 3900-2B resin. AS4 carbon fiber overwraps surround the rod. The frame stiffeners in the other direction are foam filled hats filled with Rohacell foam WF 110. A slot is cut into the frame to let the rod-stiffener pass through, and is called a keyhole. A sketch of the intersection of the two PRSEUS stiffeners is shown in figure 1 and a PRSEUS compression-loaded panel is shown in figure 2. A single frame specimen was cut from this panel to be used to verify the accuracy of the baseline analysis.

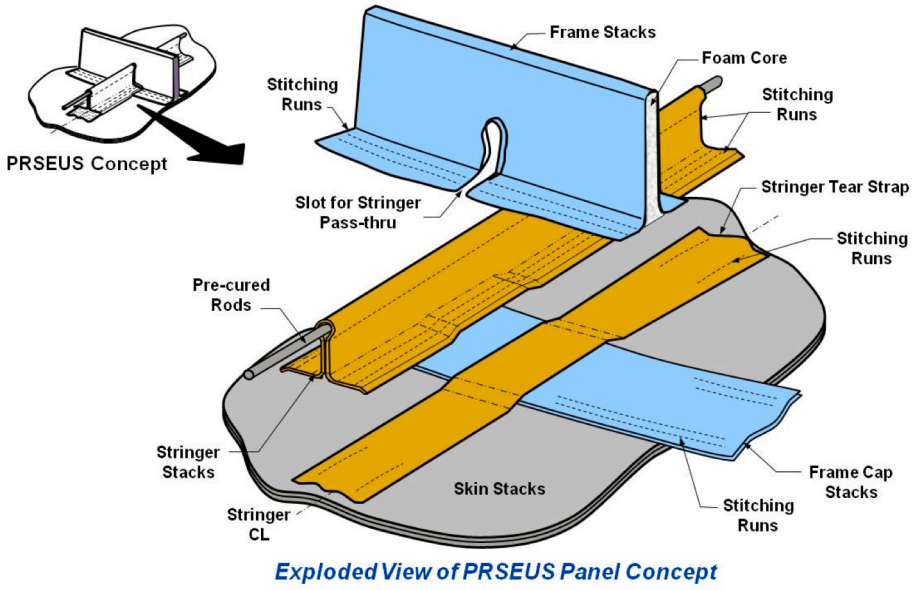

Figure 1. Intersection of PRSEUS stiffeners.

The intersection of the rod-stiffener and frame-stiffener was identified as a critical location in failure of the compression loaded two-frame panel discussed in reference [2]. There were two primary objectives of that test. The first was to evaluate the bucking and post-bucking behavior of the panel with a minimum gage thickness skin, and the second was to evaluate the failure. The panel supported load well past the buckling of the skin between the stiffeners, and the buckling behavior had little influence on the eventual failure in the stiffened regions since delaminations between the skin and flanges were prevented by the stitching and the frames did not buckle. However, the final failure of the panel ran through the keyhole location where the rod region of the stringer passes through the frame. Analysis indicated that this keyhole location had high strains due to the discontinuity. A photograph of the failure of this panel is shown in figure 3. The objective of the present study is to evaluate simple ways to reduce the stress concentration at the keyhole region.

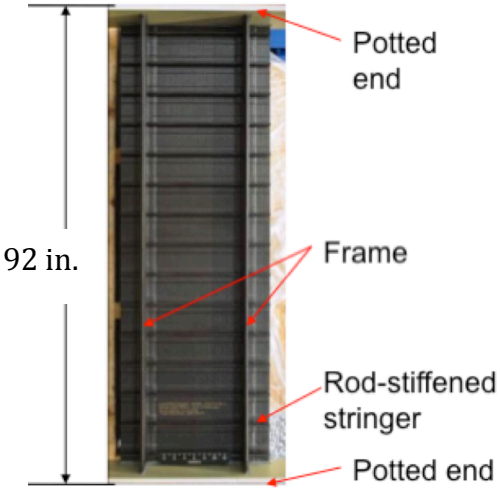

Figure 2. PRSEUS panel.

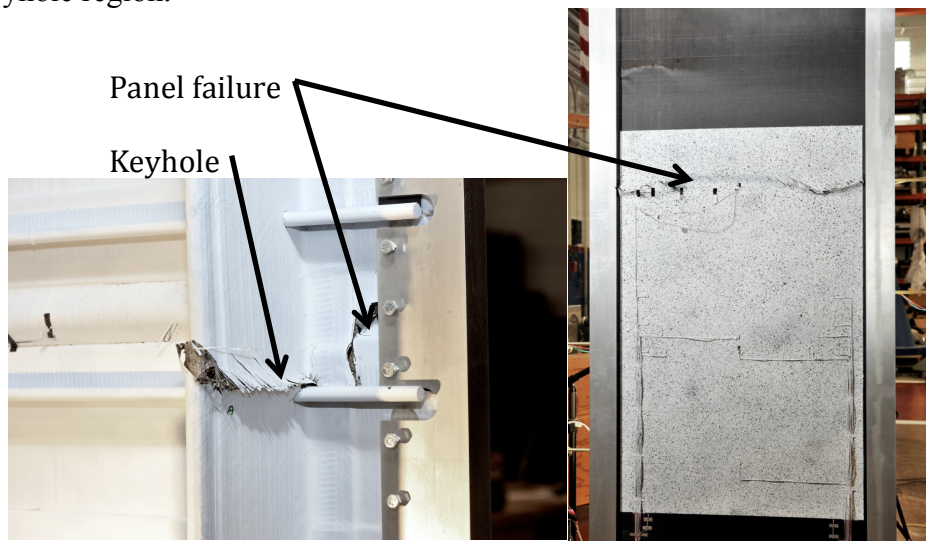

Figure 3. Panel failure through keyhole.

TEST SPECIMEN DESCRIPTION

One single-frame PRSEUS specimen was cut from the undamaged area of the compression panel shown in figure 2. The specimen was cut to 16.5 inches long with the frame-stiffener aligned in the loading direction. Two rod-stiffeners were perpendicular to the frame-stiffener. The specimen was cut three inches wide, less than the flange width. The test specimen is shown in figure 4. The geometry of the frame is shown in figure 5, where the skin and flanges are shown separately, although there is no skin-only region in the current test specimen. The skin of each specimen was one stack of material with the 0-degree orientation aligned with the stiffener. Rod-stiffeners had a 3.4-inch wide flange, a 0.104 inch-thick stiffener web and a 1.5-inch tall stiffener. The nominal diameter of the pultruded rod was 0.375 inches and the nominal thickness of the overwrap was 0.052 inches. Flange thickness was half the web thickness. One stack of additional material was added under each flange and labeled as a tear strap for the rod-stringer and a cap for the frame, as identified in figure 2. Both the tear strap and cap covered the same area of skin as the stiffener flange. Prior to testing, each end of the specimen was potted in 1.0-inch-deep epoxy compound and the ends were ground flat and parallel to each other to ensure uniform load introduction.

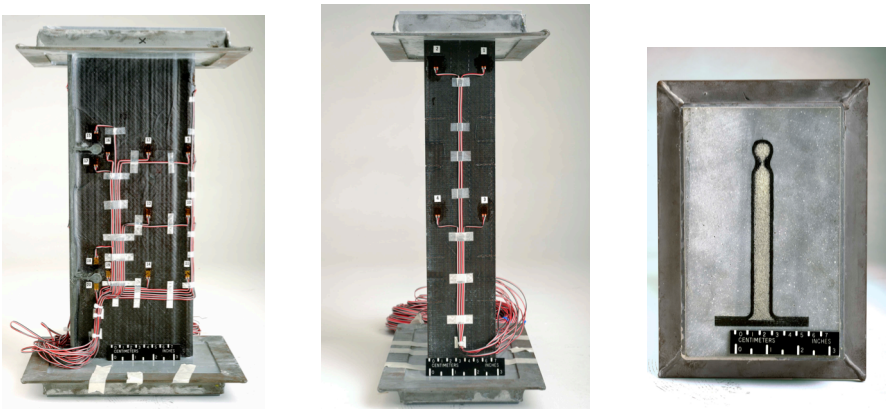

a) Frame b) Skin c) Cross section

Figure 4. Test specimen.

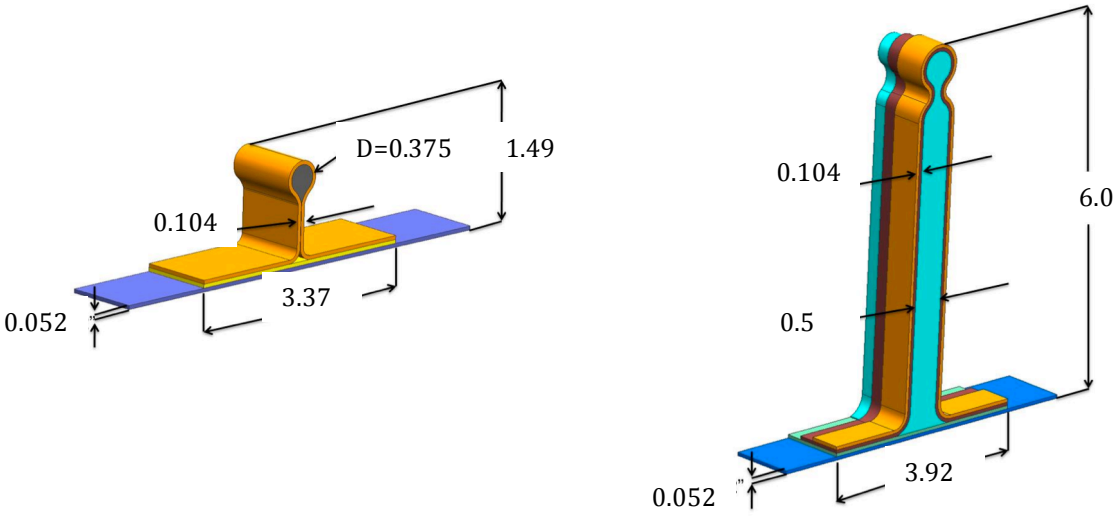

a) Rod-stiffener b) Frame

Figure 5. PRSEUS stiffeners. All dimensions are in inches.

TEST PROCEDURE AND INSTRUMENTATION

The single-frame specimen was loaded to failure in axial compression at a rate of approximately 0.005 in./minute in a 100,000 lb load frame. Displacement and strain gage data were recorded at the rate of 5 Hz as load was applied. Displacements were measured using three displacement transducers to determine end-shortening. Twenty strain gages were added to the specimen, as shown in figure 4. A specimen in the test machine is shown in figure 6. Buckling and failure behavior were noted.

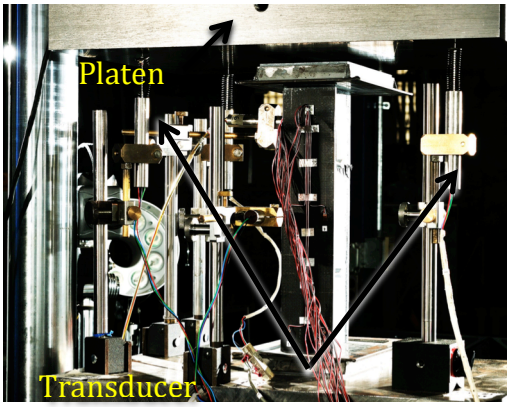

Figure 6. Specimen in test machine

ANALYSIS APPROACH

Finite element analyses of the PRSEUS specimen were conducted to compare analytical results to the test data. The model was then modified to determine the local and global effects of adding reinforcements at the stiffener intersection. The test specimen configuration will be referred to herein as the baseline arrangement. The analyses were conducted using the finite element code STAGS [3]. When only global behavior must be captured, the rod-overwrap region can be modeled as beam elements and the cutout in the frame need not be modeled in any detail. This approach has been used to capture skin buckling behavior and global deformations

and strains [1,2,4,5]. However, details must be modeled more accurately to capture the stress concentrations in the frame.

In the physical specimen, the intersection of the frame-stiffener and rod-stiffener is defined by the bond between these components and the tight fabrication tolerances where the rod-overwrap runs through the keyhole in the frame. There are no fibers or stitches crossing this intersection above the flange, but the components are cured together at the intersection. The physical proximity means the stiffeners are not independent but load cannot be guaranteed to transfer between them as if they were one piece. For a compressive load along the frame, the rod-stiffener moves with the frame and skin but has little effect on the frame behavior. For that reason, the most conservative approach is to model the specimen with no shared nodes between the rod-overwrap and the frame or between the frame and web, or to remove the rod-overwrap elements completely, leaving an open hole in the frame. The web and the rod-overwrap are continuous and pass through the frame as a single piece of structure so it is modeled as such. Ultimately, the stress concentrations directly above the keyhole are the critical stresses to consider so the keyhole can be modeled as an open hole.

Several models were considered. First, the test specimen was modeled using ½-inch per side quadrilateral shell elements for the skin, flange and web regions, with beam elements for the rod and overwrap. These beam elements were attached to the top of the stiffener web using rigid links. This coarse model was used to determine global behavior, but did not model the keyhole so stress concentrations around the keyhole could not be accurately evaluated. Second, the shell element size was reduced to ¼-inch per side while retaining beam elements for the rod-overwrap. The keyhole was still not included in this medium mesh model. Third, the beams were replaced by solid elements for the rods and overwraps. Finally, the element size was reduced to 1/8-inch per side and the shell elements in the frame were replaced with STAGS sandwich elements (8-node solid elements). The coarsest model contained 5346 degrees of freedom while the most accurate refined model contained 74,490 degrees of freedom. These finite element models are shown in figure 7, where figure 7c represents the case where the frames are represented by standard shell elements or sandwich elements. A close-up of the keyhole area is shown in figure 8 for the 1/8-inch mesh model with the rod-stiffener in place and with the rod-overwrap elements and web elements removed. Note that the geometry of the slot (approximately 0.104-inch-wide slit) through the frame through which the web passes is not modeled. Instead, the nodes in the web are independent of the nodes in the frame where the stiffeners intersect even when the nodes are co-located. Similarly, frame nodes are duplicated (but co-located) at the slot location to simulate the slot without modeling it in detail.

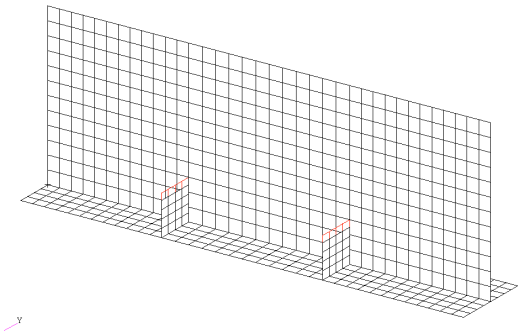

a) Coarse mesh model with bar elements

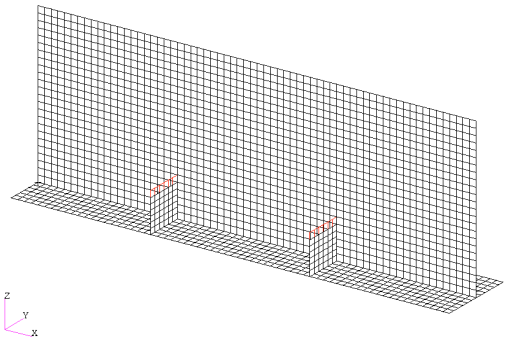

b) Medium mesh model with bar elements

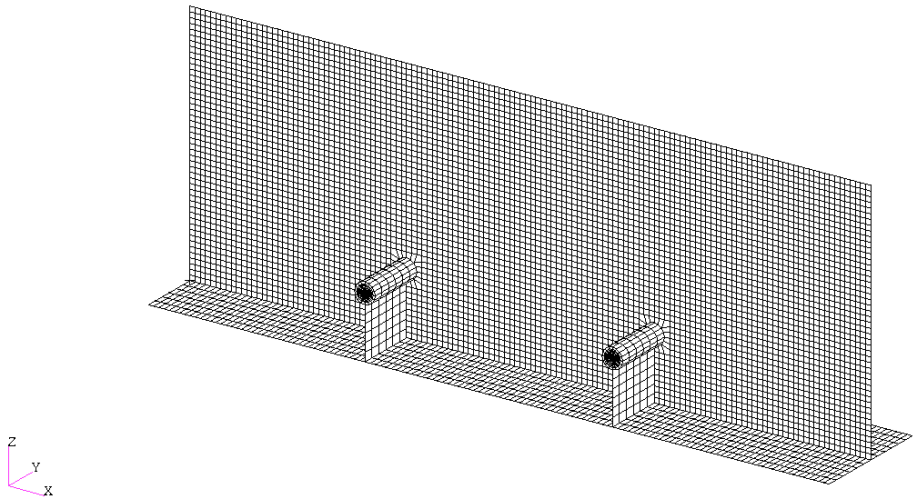

c) Fine mesh model with solid elements

Figure 7. Finite element models of baseline specimen.

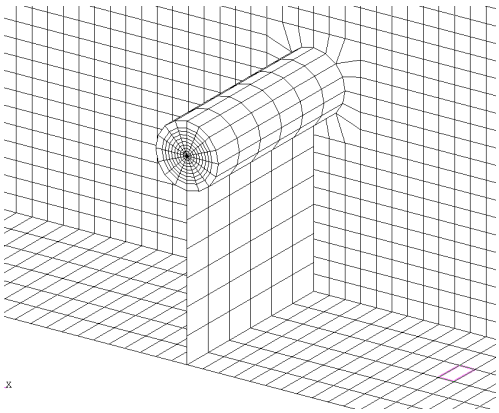

a) With stringer in place

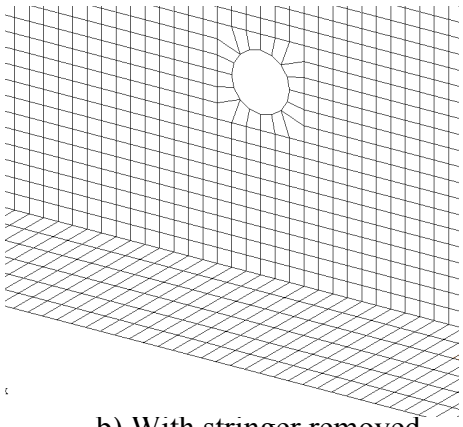

b) With stringer removed

Figure 8. Close-up of keyhole region

The 1/8-inch mesh is used in the most accurate model and is used to evaluate reinforcements in the region of the keyhole through a parametric study. However, to simplify the analysis, the solid elements were removed, leaving an open cutout in the frame. Two areas of reinforcement around the keyhole were considered to alleviate the stress concentrations. The first was a reinforcement modeled by adding carbon-epoxy material to elements within ¼-inch of the keyhole and the second by adding carbon-epoxy material to elements within 3/8-inch of the keyhole. The reinforcement regions are shown in figure 9 where the reinforcement region is shaded in yellow.

To simulate test conditions, all degrees of freedom on one end of the specimen were restrained. For a region of one inch from each end, i.e., inside the potted region, all degrees of freedom were restrained except for the shortening of the specimen. A load was applied on one end of the specimen and all nodes on that end were constrained to move the same amount to enforce uniform end shortening. The unloaded edges were unrestrained in the experiment so they were not restrained in the analysis. The potting material was not explicitly modeled.

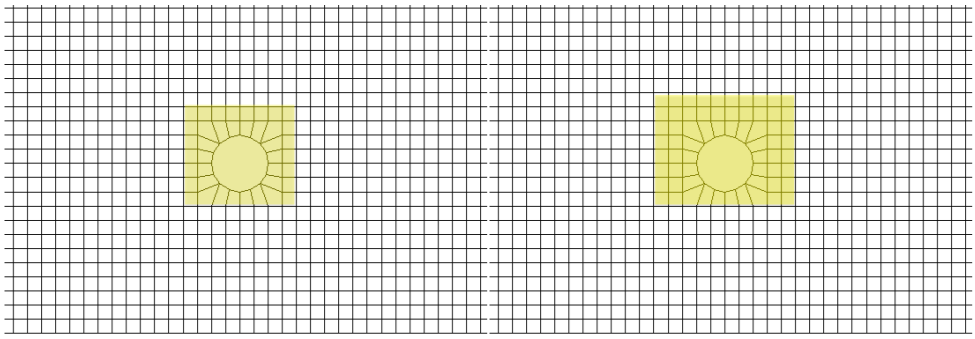

a) 1/4-inch reinforcement b) 3/8-inch reinforcement

Figure 9. Reinforcement area.

Assumed in-plane properties for the baseline configuration are based on the standard stack of material, Rohacell foam and pultruded rod and are shown in table 1 [1]. Reinforcements are assumed to be constructed from the standard stack material or several plies with different ply orientations using the ply properties presented in reference [6]. In-plane ply properties are also shown in table 1. Through-thickness properties are not as well documented, so stiffnesses for stack and 0-degree plies were assumed to be 1.0 Msi, and the shear modulus was assumed to be the same as the transverse shear modulus. The foam is assumed to be isotropic, so the properties in the thickness direction are assumed to be the same as in the transverse direction. The stacking sequences considered for the reinforcement in the parametric study are shown in table 2.

Buckling loads and geometrically nonlinear behavior were calculated for each model. Global behaviors such as end-shortening, skin strain midway between the rod-stiffeners and frame strains away from the stiffener intersections were evaluated for each model. Local strains in the vicinity of the keyhole were evaluated using only the fine-mesh model with solid elements for rods and sandwich elements for the frame.

TABLE 1. Nominal In-plane Material Properties

Property	Stack*	Foam	Rod	0-deg ply
Longitudinal stiffness, Msi	9.23	.0261	18.0	16.43
Transverse stiffness, Msi	4.66	.0261	1.0	1.60
Shear stiffness, Msi	2.26	.0102	6.0	0.80
Poisson's ratio	0.397	0.29	0.2	0.34

*Stitched stack, 0.052 inches thick, [44/44/12] percent 0/45/90

TABLE 2. Reinforcements

Label	Insert stacking sequence	Insert width (in.)*	Insert thickness (in.)
Baseline	NA	NA	NA
S-052	stack	0.25	0.052
45-04	$[\pm 45]_{2s}$	0.25	0.04
45-08	$[\pm 45]_{4s}$	0.25	0.08
Q-06	$[\pm 45_2/0/90]_s$	0.25	0.06
Q-12	$[\pm 45_2/0/90]_{2s}$	0.25	0.12
45-08L	$[\pm 45]_{4s}$	0.375	0.08
Q-12L	$[\pm 45_2/0/90]_{2s}$	0.375	0.12

* See fig. 9

RESULTS AND DISCUSSION

Experimental and analytical displacement and strains for the baseline specimen are presented to establish the accuracy of the model. Then, the results of the parametric study of reinforcements to the frame at the keyhole are shown.

Baseline configuration

The PRSEUS specimen was loaded in axial compression to failure. The failure load was 72,819 lb. The skin-flange region did not buckle in a local mode and the frame did not buckle, which would have caused a global failure. The global behavior is captured in the end shortening of the specimen as a function of load, in the measured strains at the mid-length location in the skin-flange area, and in the frame away from the keyholes. The shortening of the specimen is shown in figure 10 and far field strains are shown in figures 11 and 12. Results for the four versions of the baseline analytical model are also shown in figures 10 - 12 to demonstrate the

ability of the simpler models to accurately capture the global behavior. Experimental results are shown as solid black lines. Analytical results are shown as dashed lines. The global analytic results are similar regardless of the use of beam or solid elements for the rod region and for mesh sizes between 1/8- and 1/2-inch per side and whether the frame is modeled as shell elements or as sandwich elements. Note that for load less than 30,000 lb, excellent agreement can be seen between test and analysis. For load greater than 30,000 lb, nonlinear behavior becomes more pronounced and minor failures may be occurring.

Predicted buckling loads for the four models are within 1% of each other and are more than 3 times the specimen failure load. The analytical bucking mode is shown in figure 13, however bucking is not a contributing factor in the analytical results for the load levels corresponding to test. This bucking mode corresponds to buckling of the frame, which did not occur in the test.

Shortening of the entire specimen from the most detailed analysis is shown in figure 14 and shows a uniform behavior with little effect of the keyholes. Axial strain of the frame from the same analysis is shown in figure 15. Strain concentrations are local to the area of the keyhole. Note that the rod, overwrap and web elements are shown in red and the strains in these elements do not represent real axial strains.

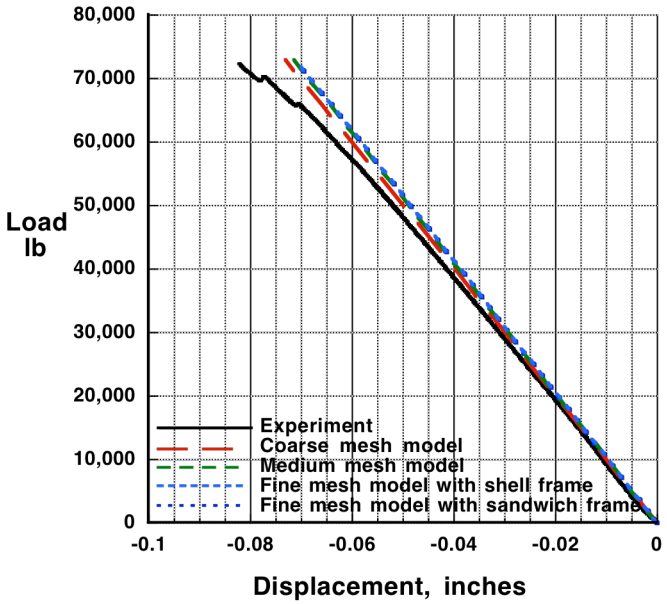

Figure 10. End-shortening for baseline configuration.

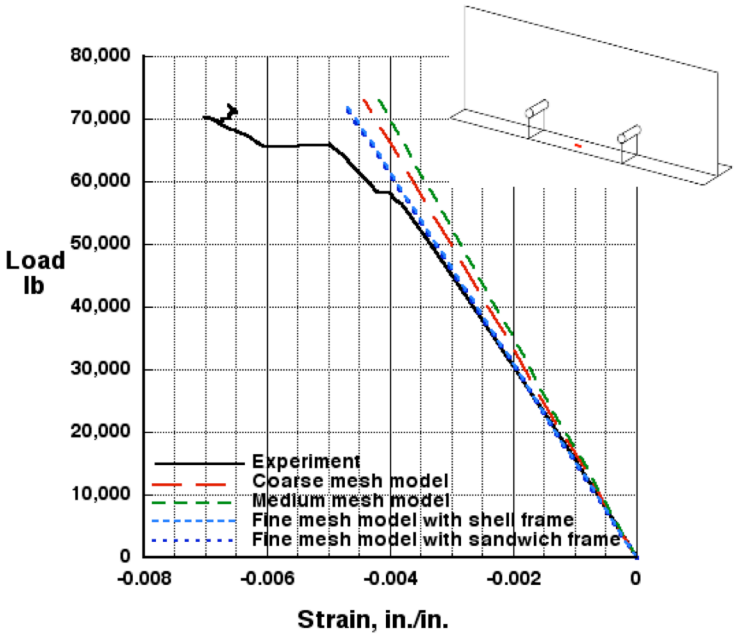

Figure 11. Axial strain in skin for baseline configuration.

Strain at a location 0.3 inches above the keyhole is shown in figure 16 for experiment and the baseline analysis where the keyhole is modeled. This result shows that strain at this point is the same whether the frame is modeled as shell or sandwich, and results in a slightly greater strain than measured in the test specimen.

The failure of the test specimen is shown in figure 17. The failure runs through the intersection of the top rod-stiffener and the full height of the frame and across the skin, resulting in edge delaminations.

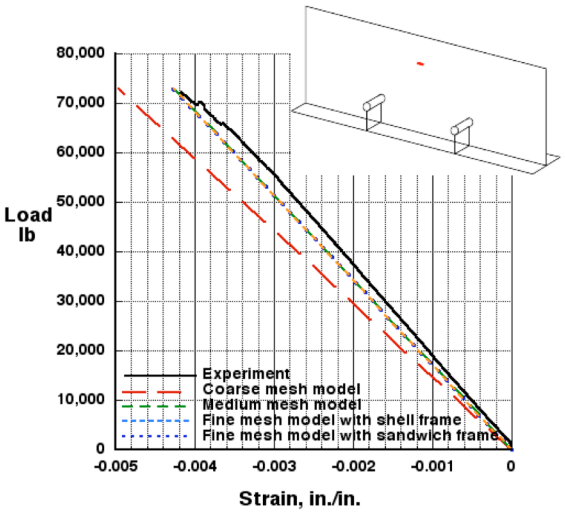

Figure 12. Axial strain in frame for baseline configuration.

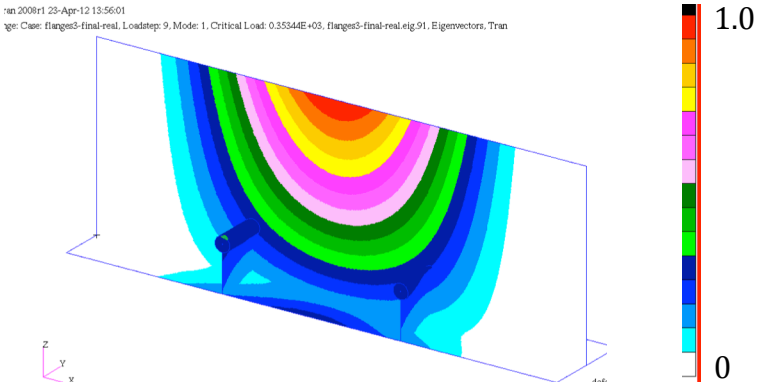

Figure 13. Buckling mode.

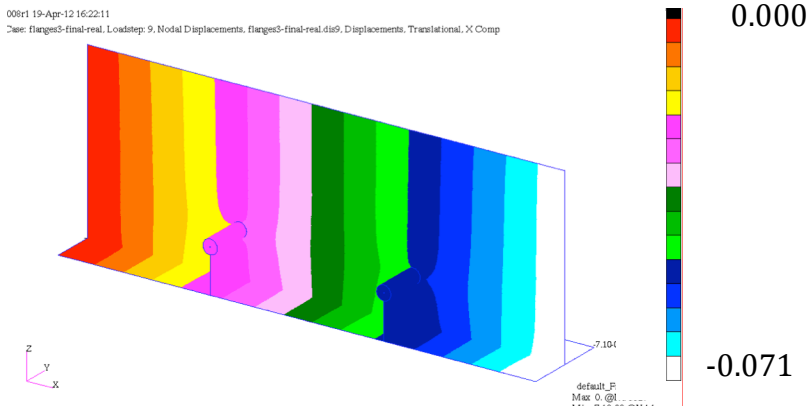

Figure 14. Displacement of baseline configuration for fine-mesh model.

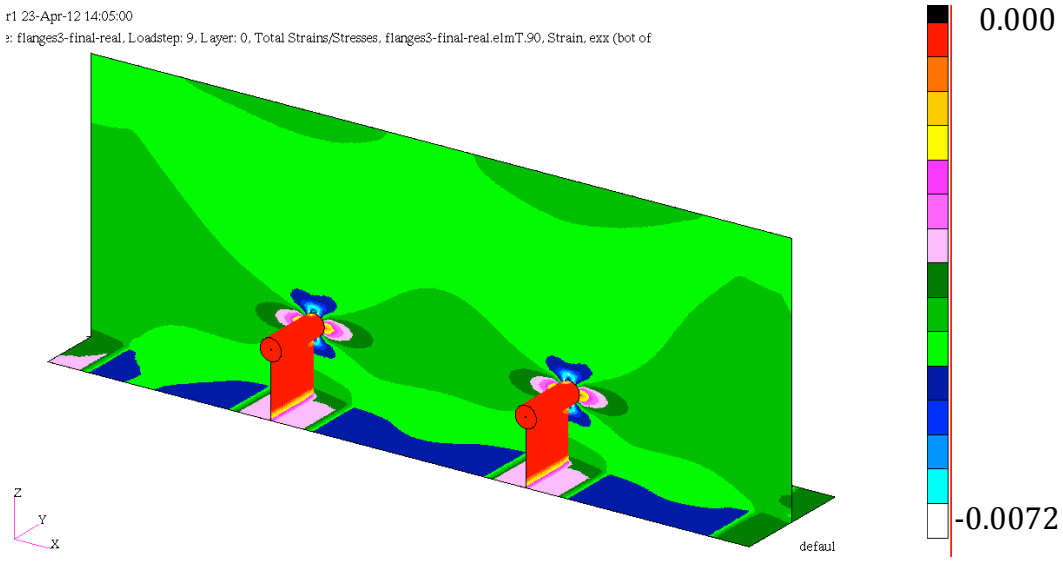

Figure 15. Axial strain in frame of baseline configuration for fine-mesh model.

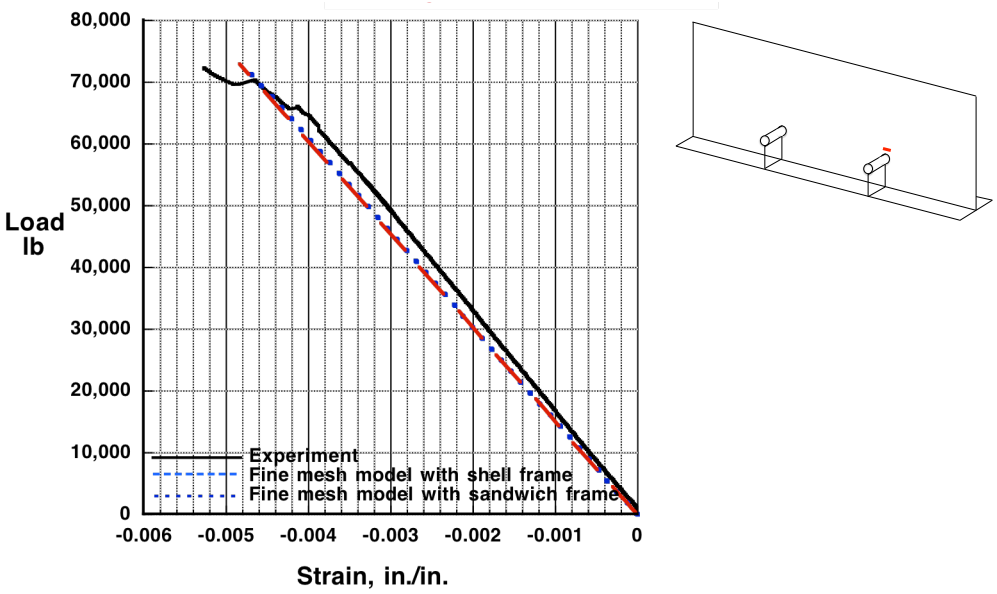

Figure 16. Axial strain 0.3 inches above keyhole.

a) Skin failure

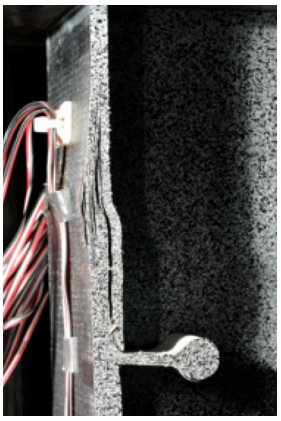

b) Edge delamination

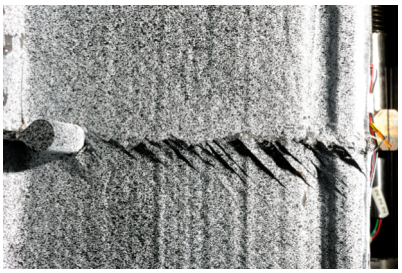

c) Frame failure

Figure 17. Failure of test specimen

Reinforcement

The fine mesh sandwich model was used to add reinforcements to the frame around the keyhole to reduce the stress concentrations in this region. These reinforcements represent inserts added between the foam and the face sheet of the sandwich frame. Foam thickness was reduced to accommodate the extra plies of material so that the face sheet would remain smooth. Inserts were added against each face sheet to keep the frame symmetric. Six stacking sequences and two reinforcement regions were considered, as described in table 2 and figure 9, respectively.

Global behaviors for the baseline configuration and seven reinforcements are shown in figures 18 through 20. In each of these figures, the baseline configuration is shown as a solid black line while reinforcements are shown as dashed lines where the color corresponds to the stacking sequence of the insert. Long dashes correspond to the ¼-inch insert and short dashes correspond to the 3/8-inch inserts. The end shortening of the baseline configuration is 0.0723 inches and the largest reduction in end shortening is with the addition of a stack of reinforcement, which causes the shortening to decrease by approximately 4.6%. Similar reductions in strain are seen far field.

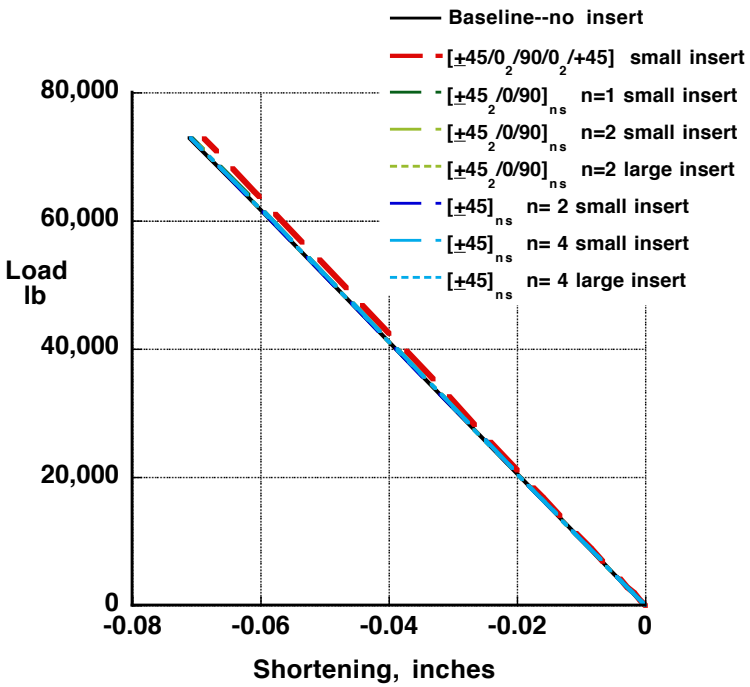

Figure 18. Calculated end shortening of baseline and reinforced specimens.

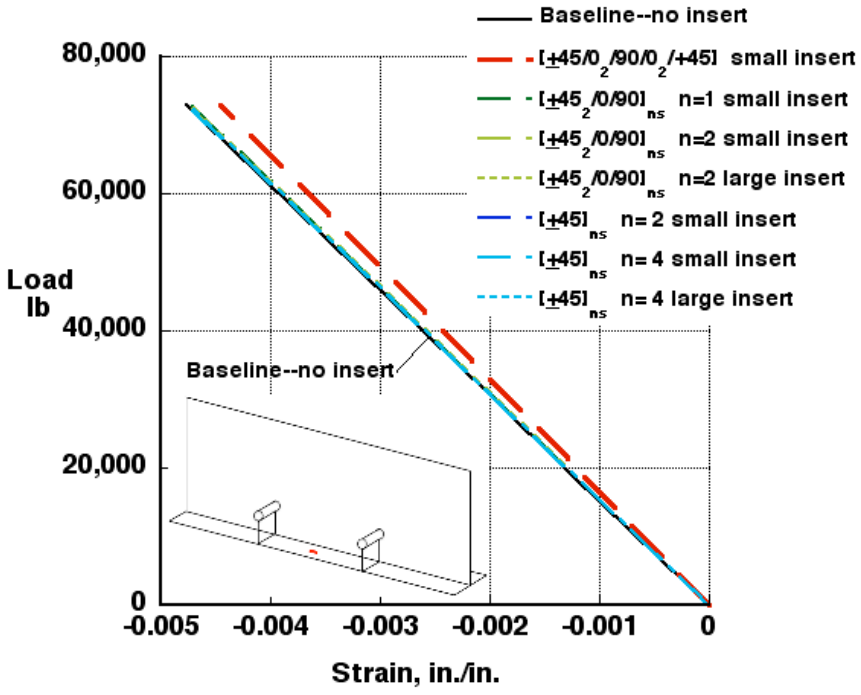

Figure 19. Calculated skin axial strain of baseline and reinforced specimens.

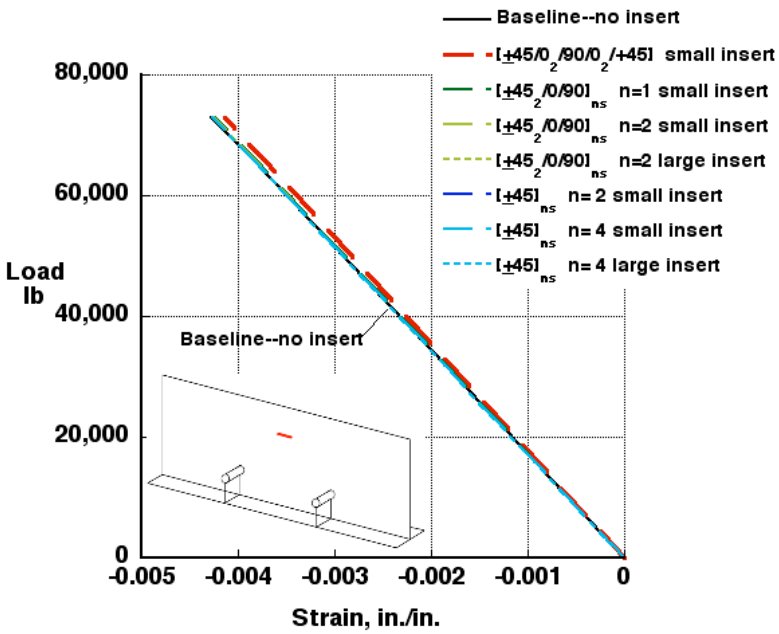

Figure 20. Calculated far field frame axial strain of baseline and reinforced specimens.

Local behavior around the keyhole is shown in figures 21 – 29. Axial strains for all inserts are shown at the location 0.3 inches above the keyhole as a function of load in figure 21. The largest reduction in strain at this location is for when the insert stacking sequence contains plies in the 45, 0 and 90 directions, but with ±45 degree plies dominating. The peak strain for each of the inserts is given in table 3.

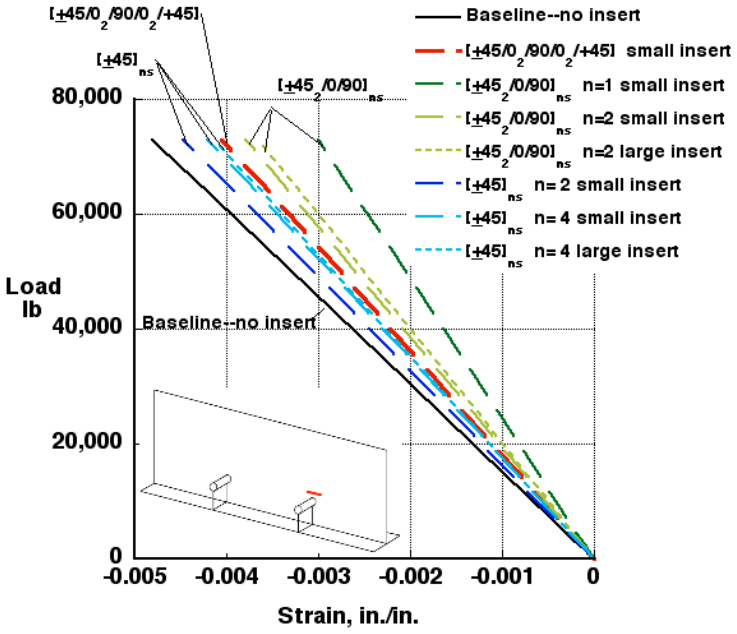

Figure 21. Calculated axial strain above keyhole of baseline and reinforced specimens.

Fringe plots in the frame near the keyhole for the baseline model is shown in figure 22 and fringe plots for all inserts are shown in figures 23-29. These full-field plots of axial strain for inserts are shown to demonstrate the range of results of strain patterns and magnitudes. The same scale is used in each of these figures for ease of comparison. Note that the location of peak strain is at the top of the keyhole cutout for all reinforcements, except where the stacking sequence is $[\pm 45_2/0/90]_s$ where the peak has moved to the edge of the reinforcement, but the magnitude has not reduced. The peak strain has decreased the most for the cases where a stack is used as the reinforcement and when a $[\pm 45_2/0/90]_{2s}$ laminate is used. A reduction of over 17% in the local peak strain is seen in both these cases. These results indicate that the thickness of the reinforcement and the size of the reinforcement is less important than the stacking sequence.

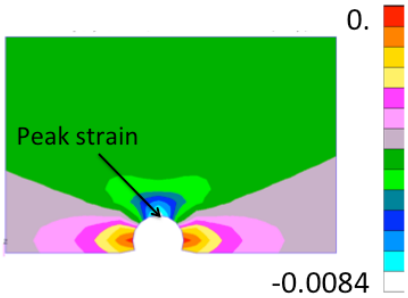

Figure 22. Baseline model axial strain in frame near keyhole.

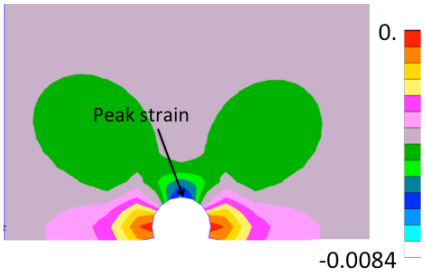

Figure 23. Model S052 axial strain in frame near keyhole.

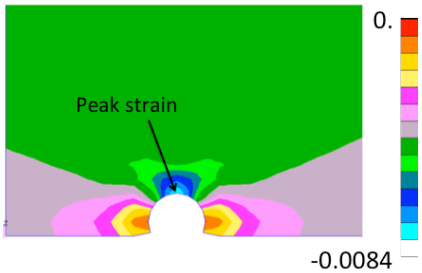

Figure 24. Model 45-04 axial strain in frame near keyhole.

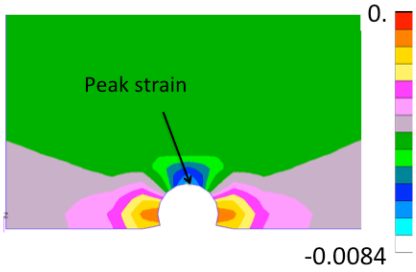

Figure 25. Model 45-08 axial strain in frame near keyhole.

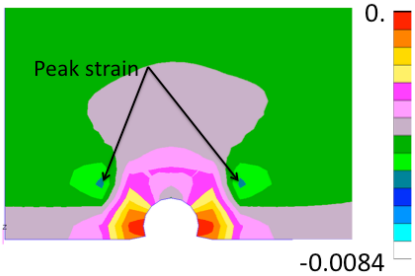

Figure 26. Model Q-06 axial strain in frame near keyhole.

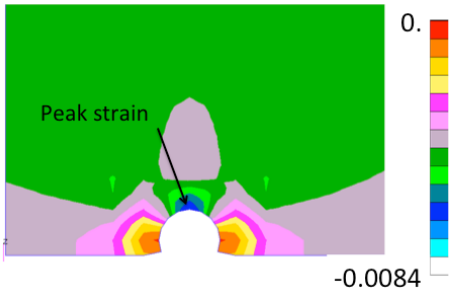

Figure 27. Model Q-12 axial strain in frame near keyhole.

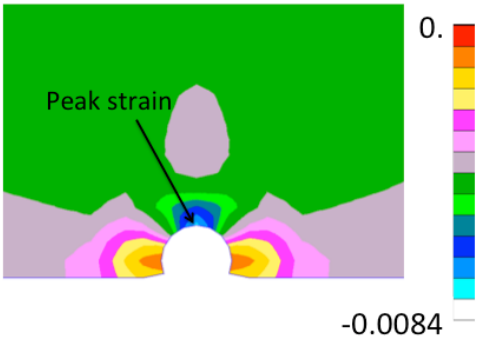

Figure 28. Model 45-08L axial strain in frame near keyhole.

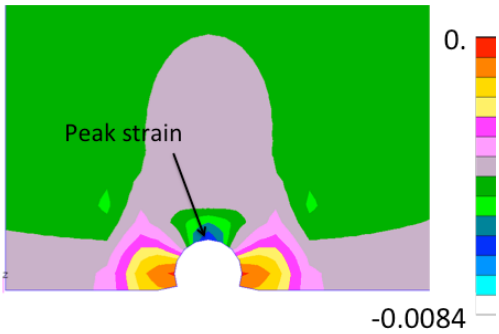

Figure 29. Model Q-12L axial strain in frame near keyhole.

TABLE 3. Peak strains in frame at cutout.

Label	Insert width (in.)	Insert thickness (in.)	Insert stacking sequence	Peak axial strain (in./in.)
Baseline	NA	NA	NA	0.00832
S-052	0.25	0.052	stack	0.00690
45-04	0.25	0.04	$[\pm 45]_{2s}$	0.00784
45-08	0.25	0.08	$[\pm 45]_{4s}$	0.00751
Q-06	0.25	0.06	$[\pm 45_2/0/90]_s$	0.00834
Q-12	0.25	0.12	$[\pm 45_2/0/90]_{2s}$	0.00688
45-08L	0.375	0.08	$[\pm 45]_{4s}$	0.00740
Q-12L	0.375	0.12	$[\pm 45_2/0/90]_{2s}$	0.00679

Based on an assumed density of 0.057 lb/in.^{3}, the reinforcement that reduces the peak strain by 17% only weighs 0.0007 lb for each intersection. In places where the stress concentrations are large enough to induce a failure, this study shows that adding a small reinforcement will reduce the strains, and therefore could delay the onset of failure.

APPLICATION TO FULL SCALE PANELS

This analysis can provide insight into the behavior of the keyhole region in larger structures. If the best reinforcement considered in this study were added to all stiffener intersections in the original panel (see figure 2), the panel weight would increase slightly. Based on an assumed density of the reinforcement of 0.057 lb/in.^{3}, the heaviest reinforcement (Q-12L) adds 0.02 lb per intersection but lowers the peak strain by 17%. Since the anticipated aerial weight of a typical PRSEUS panel is 2.1 lb/ft^2 [1], this reinforcement would increase the aerial weight of the panel by less than 0.01%. The added weight is quite small but the additional manufacturing effort of hollowing out the foam to the correct size and adding the reinforcement could limit its application to critical intersections. In the full-scale 2-frame compression panel discussed herein, there were strain concentrations at the keyhole of approximately the same magnitude as at the panel

edges and at some flange edges. Stress concentrations at these locations would also have to be addressed to have a significant impact on panel behavior.

CONCLUDING REMARKS

The strains at the intersection of the stiffeners in a Pultruded Rod Stitched Efficient Unitized Structure (PRSEUS) panel are evaluated. An analytical parametric study demonstrates that adding reinforcements locally to a very small area of the intersection can significantly reduce the strain concentration. This approach could be used to increase a panel failure load without appreciably increasing the panel weight.

REFERENCES

1. Velicki, A., "Damage Arresting Composites for Shaped Vehicles," NASA CR-2009-215932.
2. Yovanof, N and Jegley, D., "Compressive Behavior of Frame-Stiffened Composite Panels," presented at the 52nd AIAA/ASME/ASCE/AHS Structures, Dynamics and Materials Conference, Denver, CO, April 2011.
3. Rankin, C. C., Loden, W. A., Brogan, F. A, and Cabiness, H. D., "STAGS Users Manual," Rhombus Consultants Group, Inc., Palo Alto, CA, 2007.
4. Przekop, A., "Repair Concepts as Design Constraints of a Stiffened Composite PRSEUS Panel," Proceedings of the 53rd AIAA/ASME/ASCE/AHS/ASC Structures, Structural Dynamics and Materials Conference, Honolulu, HI, April, 2012.
5. Jegley, D., "Structural Efficiency and Behavior of Pristine and Notched Stitched Structure," presented at SAMPE Fall Technical Conference, Fort Worth, TX , Oct. 2011.
6. Jegley, D., " Improving Strength of Post-Buckled Panels Through Stitching," Journal of Composite Structures. Vol. 80, pp 298-306, 2007.